

Experimental study of the convection in a rotating tangent cylinder

Kélig Aujogue¹, Alban Pothérat², Binod Sreenivasan³ and François Debray⁴

¹ School of Chemical Engineering, University of Birmingham, Edgbaston, Birmingham B15 2TT, UK ² Applied Mathematics Research Centre, Coventry University, Prior Street, Coventry CV15FB, UK ³ Centre for Earth Sciences, Indian Institute of Science, Bangalore 560 012, India. ⁴ Laboratoire National des Champs Magnétiques Intenses-Grenoble, CNRS/UGA-UPS-INSA, France

(Received 28 March 2017)

This paper experimentally investigates the convection in a fast rotating Tangent Cylinder (TC), for Ekman numbers down to $E = 3.36 \times 10^{-6}$, in a configuration relevant to the liquid core of the Earth. In the apparatus, the TC results from the Proudman-Taylor constraint incurred by rotating a hemispherical fluid vessel heated in its centre by a protruding heating element of cylindrical shape. The resulting convection that develops above the heater, *i.e.* within the TC, is shown to set in for critical Rayleigh numbers and wavenumbers respectively scaling as $Ra_c \sim E^{4/3}$ and $a_c \sim E^{1/3}$ with the Ekman number E . Though exhibiting the same exponents as for plane rotating convection, these laws are indicative of much larger convective plumes at onset. The structure and dynamics of these plumes are in fact closer to those found in solid rotating cylinders heated from below, suggesting that the confinement within the TC induced by the Taylor-Proudman constraint influences convection in a similar way as solid walls would do. There is further similarity in that the critical modes in the TC all exhibit a slow retrograde precession at onset. In supercritical regimes, the precession evolves into a thermal wind with a complex structure featuring retrograde rotation at high latitude and either prograde or retrograde rotation at low latitudes (close to the heater), depending on the criticality and the Ekman number. Nevertheless the intensity of the thermal wind measured by the Rossby number scales as $Ro \sim 0.85(Ra_q^*)^{0.41}$ with the Rayleigh number based on the heat flux Ra_q^* . This scaling suggests that the convection in the TC is driven by quasi-geostrophic dynamics, a finding supported by the scaling for the rotation-normalised Nusselt number $Nu^* \sim (Ra_q^*)^{5/9}$.

Key words: Rapidly rotating convection, planetary interiors, tangent cylinder, Proudman-Taylor constraint, spherical shells, quasi-geostrophic flows.

1. Introduction

This paper is concerned with convective flows confined in a cylindrical region by the action of the Taylor-Proudman (TP) constraint due to background rotation. Our prime motivation comes from the study of liquid planetary cores such as the Earth's. In the Earth's interior, the liquid core occupies a 2200 km-thick region between the solid iron inner core (1200km in radius) and the 3000-km thick rocky mantle (Fig. 1). Heat and solute elements released from the solid core drive thermal and compositional convection, which is in turn shaped by both the planet's fast rotation and its magnetic field. Because

of the very fast rotation of the Earth (Ekman numbers down to 10^{-15}), The Taylor-Proudman constraint creates an imaginary boundary in the shape of a cylinder tangent to the solid inner core and extending up to the Core-Mantle Boundary, which opposes exchange of fluid between regions inside and outside it. Consequently, the region inside the TC is subject to intense convection but also to an important effect of confinement of a different nature to that imposed by solid walls.

Until now, convection in TCs has been tackled from three different angles: linear stability analyses mostly focused on the interplay between convection and rotation in plane geometries, where the TP constraint is absent. Early results, reviewed in Chandrasekhar (1961)'s monograph, showed that under the effect of rotation, the critical Rayleigh number for the onset of convection increased as $Ra_c \sim E^{-4/3}$ while convective cells became thinner, with their wavenumber increasing as $a_c \sim E^{-1/3}$ (Here the Ekman number $E = \nu/2\Omega h^2$ is build with the background speed of rotation Ω , fluid viscosity ν and the height of the fluid layer h). An important feature of plane rotating convection is that for a Prandtl number beyond a few units (0.677 for free-slip boundaries), the unstable mode at onset does not oscillate (*i.e* convection is not overstable, see Clune & Knoblauch (1993)). Other theoretical approaches treated spherical shell geometries, following the seminal work of Busse (1970) but since convection outside the TC ignites at much lower Rayleigh numbers than inside the TC, these works mostly focused on that part of the core rather than the TC.

Numerical simulations in planetary geometries provided key insight into the global dynamics of liquid core including the effect of the TP constraint, even though none were specifically dedicated to the TC. Aubert (2005) and Christensen & Aubert (2006) showed that the heat flux from the Inner Core boundary (ICB) to the Core Mantle Boundary (CMB) obeyed a somewhat universal scaling of the form $Nu^* = 0.076(Ra_q^*)^{0.53}$, when expressed in terms of the heat flux-based Rayleigh number Ra_q^* and rotation-normalised Nusselt number Nu^* (see exact definitions in Eqs. (4.4,4.6)). A similar result was obtained for the azimuthal thermal wind, which is driven by radial temperature variations between regions inside and outside the TC: its intensity measured by a Rossby number built on RMS velocity scaled as $Ro = 0.85(Ra_q^*)^{0.41}$. This scaling is consistent with Cardin & Olson (1994)'s hypothesis of potential vorticity conservation in a geostrophic regime, which translates into the very similar scaling of $Ro \sim (Ra_q^*)^{0.4}$. These scalings were obtained in dynamo simulations incorporating the full coupling between buoyancy, rotation and electromagnetic effects. Nevertheless, Aubert (2005)' numerical simulations showed that they remained valid with or without magnetic field. This suggests that both the heat flux and the thermal wind are mostly controlled by the amount of available buoyancy. While this amount may be altered by electromagnetic effects, this influence becomes transparent when the Rayleigh and Nusselt numbers are expressed in terms of the buoyancy itself. Nevertheless, these scalings are not specific to the TC and the question remains open as to whether they still stand when considering the dynamics of the TC only.

Aurnou *et al.* (2003) used dye visualisation to analyse convection in the only experiment dedicated to the TC to date. The authors identified convective structures, labelled "rim instabilities" that differ from those expected in plane rotating convection. Despite some data scattering, the authors suggest that the associated thermal wind was consistent with a scaling of the form $U \sim 2(B/(2\Omega))^{1/2}$, where B is the buoyancy flux. Unlike Cardin & Olson (1994)'s model, this scaling reflects the balance between the Coriolis force and inertia-driven convection outside the geostrophic regime Maxworthy & Narmousa (1994). However, a characterisation of the onset of rotating convection in the TC is currently lacking and it is not clear how convection is affected by the confinement

induced by the TC.

Goldstein *et al.* (1993) and Zhong *et al.* (1993) provide an insight on the question of the confinement, in the configuration of a rotating cylinder bounded by solid walls. Linear stability analysis distinguishes slow and fast convective modes, depending on the aspect ratio of the cylinder and the level of supercriticality. Importantly, in breaking translational symmetry, the presence of solid walls are shown to incur a retrograde precession at onset that always precludes the occurrence of steady modes observed in plane geometry. Nevertheless, the precessing frequencies at onset are much lower than those of oscillating modes in overstable regimes, and the associated precessing motion resembles more the retrograde thermal wind found in planetary cores than overstable travelling waves found a low Prandtl number in plane rotating convection (Chandrasekhar (1961); Clune & Knoblauch (1993)). Indeed, in more supercritical regimes (typically 10 times critical), experiments by Zhong *et al.* (1993) showed that the precession progressively led to a large retrograde structure centred in the middle of the cylinder. However, it is not clear to which extent the virtual boundaries of the TC influence the convection in the same way as the rigid boundaries of a real cylinder do ; nor is it clear whether the findings of Goldstein *et al.* (1993) and Zhong *et al.* (1993), obtained for Ekman numbers of the order of 10^{-2} extend to the much lower Ekman numbers relevant to planetary interiors. In view of these interrogations, the purpose of this paper is to experimentally analyse convection in a Tangent Cylinder at low but experimentally accessible Ekman numbers, and in particular to address the following questions:

- (a) What are the critical conditions for the onset of convection ?
- (b) Do the critical modes follow the phenomenology observed in plane or cylindrical geometries? In particular, are these modes steady ?
- (c) What do these patterns evolve to in supercritical regimes ?
- (d) How are heat transfer across the TC and the thermal wind affected by the combined influence of rotation and confinement within the TC ?

Our experiments rely on the Little Earth Experiment (LEE) facility which we designed to reproduce rotating magnetoconvection in a tangent cylinder configuration as relevant to Earth as possible Aujogue *et al.* (2016). Nevertheless, all experiments reported in this paper were conducted in the absence of magnetic field and electromagnetic effects will be the focus of later work. The layout of the paper is as follows: in section 2, we briefly describe LEE and the measurement techniques implemented in it. In section 3, we analyse convective patterns in view of answering questions (a), (b) and (c). Section 4 is dedicated to the characterisation of heat flux and the thermal wind while section 5 seeks to assess the confinement effect induced by the TC.

2. Experimental Setup

Our experimental apparatus is discussed in detail in Aujogue *et al.* (2016). Its main features are summarised on figure 1. We used a hemispherical dome of inner diameter $2R_D = 276$ mm filled with water or sulphuric acid. At the centre of the dome, a cylindrical heater of height 18 mm and diameter $2\eta R_D = 100$ mm protrudes into the dome. η is the ratio of heater to dome radii, which represents the ratio of CMB to ICB radii for the Earth. Hence the thickness of the liquid corresponds to the height of fluid above the heater at the centre of the dome $d = 120$ mm. The heater provides an isothermal boundary condition at temperature T_H on its upper surface and ensures an adiabatic boundary condition at its lateral boundary. These conditions are guaranteed by the material of the heater: ceramic for the upper surface and polytetrafluoroethylene (PTFE) for the lateral boundary. Indeed, considering the heat flux through these materials (Φ_{ceramic} and Φ_{PTFE}

respectively), we obtained a ratio of

$$\frac{\Phi_{\text{PTFE}}}{\Phi_{\text{ceramic}}} \sim 0.0061 \ll 1. \quad (2.1)$$

Therefore the flux throughout the lateral boundary can be neglected with respect to the flux throughout the upper surface. The heater operates as a heat exchanger fed at a constant flow rate by a heat-carrying fluid (Ethylene-Glycol) whose temperature is controlled in the static frame, so the heat flux F delivered to the working fluid inside the dome is obtained by measuring the temperature difference between the inlet and the outlet of the heater. The temperature at the outer surface of the dome T_D is held constant by immersing the whole system in a large volume of water. Overall, the temperature difference driving convection $\Delta T = T_H - T_D$ is controlled to within $\pm 0.2^\circ\text{C}$ and spans values within $[0.7 - 25]^\circ\text{C}$. The entire setup is rotated about the vertical axis at angular velocity Ω $[\pi - 3\pi]$ rad/s, by means of an electric motor located approximately 2.5 m below the floor of the hemispherical fluid domain. Even though we shall focus on rotating convection only in this paper, it must be kept in mind that the setup was designed to study both convection and magnetoconvection. Hence, this choice of mechanical design, which allows us to operate the setup within the bore of large resistive magnets whilst keeping the motor away from regions of high magnetic fields (Such experiments will be reported in a later paper). This way we aim to reproduce a geometry relevant to the Earth Tangent Cylinder. Although the results discussed in this paper were obtained without magnetic field, the layout of the experiment remained the same as shown on figure 1.

The working fluids were either water or sulfuric acid (H_2SO_4) concentrated at 30% mass of respective densities $\rho_{\text{H}_2\text{O}} = 1000$ and $\rho_{\text{H}_2\text{SO}_4} = 1250 \text{ kg/m}^3$, viscosities $\nu_{\text{H}_2\text{O}} = 0.9 \times 10^{-6}$ and $\nu_{\text{H}_2\text{SO}_4} = 2.06 \times 10^{-6} \text{ m}^2/\text{s}$, thermal diffusivities $\kappa_{\text{H}_2\text{O}} = 1.4 \times 10^{-7}$ and $\kappa_{\text{H}_2\text{SO}_4} = 1.7 \times 10^{-7} \text{ m}^2/\text{s}$ at 20°C . Water was chosen for ease of use, whereas sulfuric acid was chosen as the transparent fluid with a high electric conductivity, in view of future experiments in high magnetic fields.

The range of parameters in which we operated the setup is reported in table 1. The dimensionless parameters controlling the flow in the experiment are the Rayleigh number $Ra = g\alpha\Delta T d^3/\kappa$ (ratio of the buoyancy forces to the viscous friction forces), the Ekman number $E = \nu/\Omega d^2$ (ratio of the viscous forces to the Coriolis force), the Prandtl number $Pr = \nu/\kappa$ (ratio of the diffusivities).

We measure the flow velocity with a bespoke particle image velocimetry (PIV) system in three distinct planes: one the vertical plane aligned with a dome's diameter, and two horizontal planes positioned at 0.09 m and 0.02 m above the surface of the heater (see figure 1).

In the former, we measure velocity $(u_r(r, z), u_z(r, z))$, where r and z are the radial and vertical coordinates respectively, whereas we measure $(u_r(r, \theta), u_\theta(r, \theta))$ in the latter two (here and for the reminder of the paper, we use cylindrical-polar coordinates with the origin at the centre of the heater's upper circular surface).

Temperatures are monitored in real-time by means of 4 K-type thermocouples: one is placed at the outer surface of the dome, one is embedded within the top surface of the heater, and two respectively measure temperature of the heat-carrying fluid at the heater's inlet and outlet, thus providing accurate monitoring of F ($\pm 0.14 \text{ W/m}^2$). The rotating velocity is also monitored by means of an optical sensor. Technological details of the setup, and validation tests are available in Aujogue *et al.* (2016).

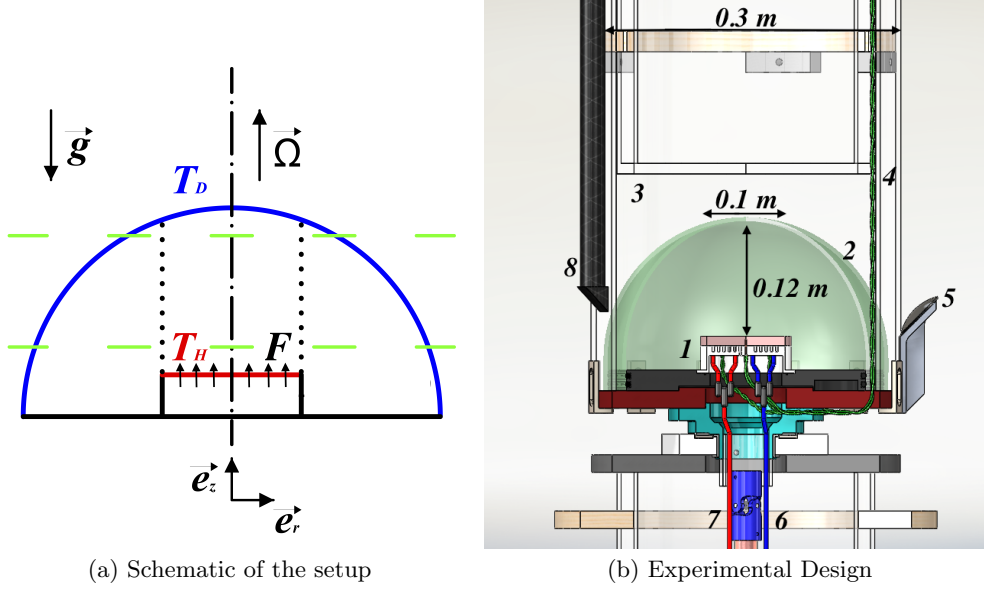


Figure 1: Left panel: Schematic of the experimental geometry in the vertical plane with T_H the temperature at the heater, T_D the temperature at the dome, Ω the rotation speed, g the gravity, and F the heat flux through the heater. The green dashed lines represent the two horizontal PIV planes. The red line is the surface of the heater. The blue line is the surface of the dome. The dashed/dotted black line is the axis of symmetry and rotation of the experiment. The dotted lines are the boundary of the Tangent Cylinder. Right panel: 1. Liquid Heater 2. Dome 3. Cooling Water 4. K-type thermocouples connected under and in the ceramic plate 5. Mirror 6. Torque tube 7. Pipe carrying ethylene glycol 8. PIV Camera. Material partially presented in Aujogue *et al.* (2016).

The experimental protocol consists of first setting a rotation rate Ω and waiting until the flow reaches a solid body rotation (typically 30 min, verified by means of PIV measurements with the heater off). We then heat the heat-carrying fluid at a prescribed temperature, until ΔT reaches a constant value. Only when the entire system has reached a statistically steady thermal and mechanical state, are the output of the thermocouples and PIV data recorded.

3. Structure of the convective patterns

3.1. Onset of convection

In this section, we focus on the flow near the onset of convection. The combined effect of buoyancy and rotation generates a flow structured in columns at the onset. This is illustrated by the contours of vertical velocity obtained for different values of E on Fig. 3. The columns are exclusively confined within the tangent cylinder, with very little fluid motion outside of this region. Columns become thinner at lower values of E , a tendency that has been previously observed both in spherical and plane geometries Sreenivasan & Jones (2006); Chandrasekhar (1961); Aujogue *et al.* (2015).

On figure 2, we show that variations of the critical Rayleigh number with E follow a

Control parameters	Water	H ₂ SO ₄	Earth core
$E = \nu/\Omega d^2$	$1.25 \times 10^{-5} - 1.25 \times 10^{-6}$	$4.51 \times 10^{-5} - 4.51 \times 10^{-6}$	10^{-15}
$Ra = g\alpha\Delta T d^3/\kappa\nu$	$2.09 \times 10^7 - 2.93 \times 10^9$	$1.4 \times 10^7 - 2.25 \times 10^9$	10^{22}
$Pr = \nu/\kappa$	7	12	10^{-2}
$\eta = R/R_D$	0.355	0.355	0.35

Table 1: Range of achievable parameters in the experiment and comparison with the Earth Core parameters: ν is the viscosity, Ω the rotation rate, d is the height of fluid above the centre of the heater, g the gravitational constant, α the expansion coefficient, ΔT the temperature difference between the heater and the dome, κ the thermal diffusivity, R_D the radius of the dome and R the radius of the heater. Note that the values of Ra for the Earth are highly uncertain (Schubert & Soderlund (2011)). Material originally presented in Aujogue *et al.* (2016)

scaling of $Ra_c \sim (26 \pm 4) \times E^{-1.31 \pm 0.05}$. Despite a very different geometry, this scaling is in very good agreement with the theoretical prediction of $Ra^c = 22.3 \times E^{-4/3}$ for rotating convection in an infinitely extended plane layer Chandrasekhar (1961). This result suggests that the critical Rayleigh number is not measurably affected by the geometry and reflects a very robust feature of rotating convection.

We shall now analyse the horizontal size of the convective structures present at the onset. Since translational invariance in the horizontal plane is lost in our geometry, we extract the horizontal size of convective structures by seeking the separation r_0 corresponding to the first zero of the spatial correlation function built from u_r , and averaged over time and z :

$$C_{u_r}(\delta r) = \left\langle \int_{\mathcal{V}} u_r(r + \delta r) u_r(r) dr dz \right\rangle_t, \quad (3.1)$$

where \mathcal{V} represents the intersection of the meridional plane lit by the PIV LASER and the TC. At the onset, the associated wavenumber $a_c = 2\pi R/r_0$ can be compared to the critical wavenumber predicted for the onset of rotating convection in an infinite plane layer (Fig. 2). In the tangent cylinder geometry, we find a scaling of

$$a_c = (0.5 \pm 0.07) \times E^{-1/3 \pm 0.05} \quad (3.2)$$

when the plane layer theory predicts $a_c = 1.65 \times E^{-1/3}$ Aujogue *et al.* (2015). Although both structure sizes exhibit the same scaling exponent, critical wave numbers are significantly lower in the tangent cylinder geometry than for the infinite plane layer. We shall see in section 3.2 that the reason for this discrepancy finds its root in the topological structure of the critical modes.

Lastly, a remarkable feature of the onset of rotating convection in plane layers is that for the values of Pr considered in this paper, the critical mode is predicted to be steady Clune & Knoblauch (1993). By contrast, in all our measurements, we found a time-dependent flow at the onset. Inspection of the flow in horizontal planes reveals that the convective plumes are subject to a retrograde precession. The variations of the corresponding frequency ω_p derived from the maximum velocity along θ in the horizontal plane and normalised by the background angular frequency

are reported on figure 6. The precession at the onset of convection and beyond has

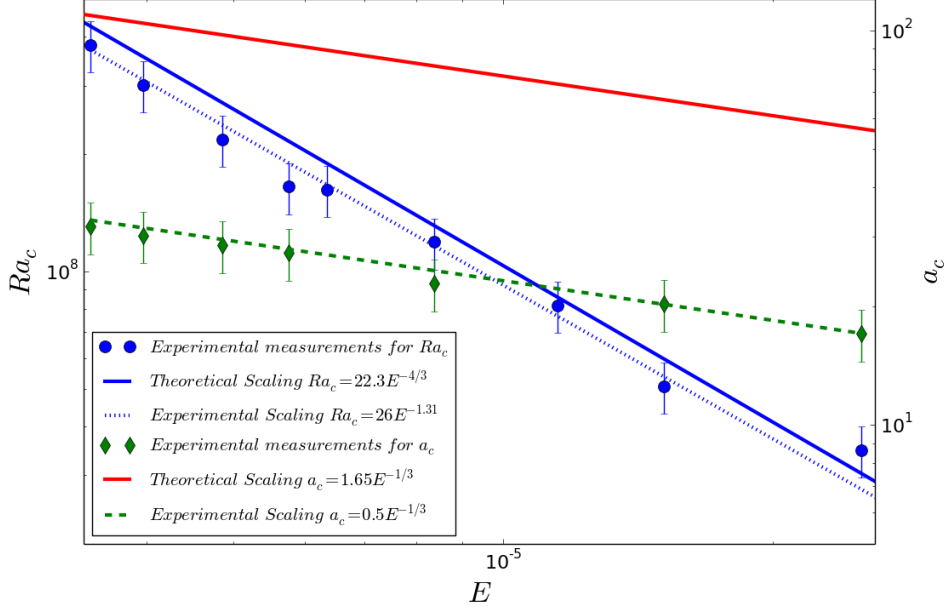


Figure 2: Critical Rayleigh number Ra_c and critical wave number $a_c = 2\pi R/r_0$ at onset *vs.* the Ekman number E .

been studied theoretically and experimentally in Goldstein *et al.* (1993) and Zhong *et al.* (1993) in rigid rotating cylinders of various aspect ratios. In these studies, the authors showed that the loss of translational symmetry in the radial direction necessarily induced a precession in the critical mode and that the corresponding frequency normalised by the background rotation Ω , ω_{p_0} obeyed a scaling of the form $\omega_{p_0} = \delta E^{-1}$.

δ was determined experimentally by Ecke *et al.* (1992) as $\delta = 0.1$ for a radius-to-height aspect ratio of $\Gamma = 1$.

Our measurements produce a value of $\delta = 0.07 \pm 0.005$. This value is close to that found by Ecke *et al.* (1992), despite a lower aspect ratio (measured at the centre of the heater) of $\Gamma = R/d = 5/12$.

In summary, the study of critical Rayleigh, plume size, and precession frequency shows that the onset of convection in a tangent cylinder corresponds to an hybrid behaviour between those of convection in an infinite plane layer and in a rotating cylinder. Certainly the scaling for the critical Rayleigh number from the plane layer theory is reproduced in the tangent cylinder but size and time-dependence of the flow are more accurately described by the phenomenology of convection in rigid rotating cylinders.

3.2. Supercritical flow patterns

We shall now explore the evolution of the patterns from the onset of convection into the supercritical regime, focusing on two values of the Ekman number $E = 1.15 \times 10^{-5}$ and $E = 6.36 \times 10^{-6}$, for critical parameters $R_c = Ra/Ra_c - 1$ up to 13. Figs. 4a to 4f illustrate the development of convective patterns for a criticality in the range $0.1 \leq R_c < 12$ and $E = 1.15 \times 10^{-5}$.

Near the onset of convection ($R_c = 0.13$, Fig.4a) we observe a behaviour reported by

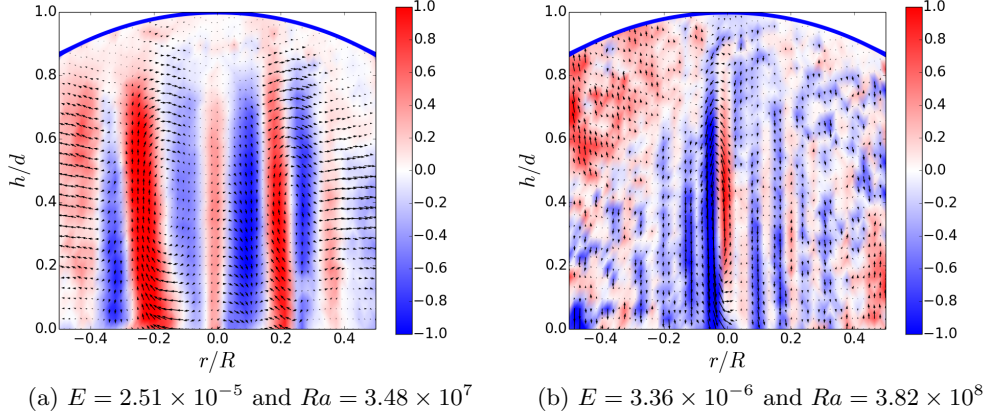


Figure 3: Average over time of the vertical component of velocity from PIV measurement above the liquid heater at the onset of convection. The averaging time is 15 times smaller than the precession timescale $\tau_p = 2\pi/\omega_p$. Velocities are normalised by the maximum velocity in the flow. z and r are normalised by the maximum height above the heater and the radius of the heater respectively. The blue line represents the inner boundary of the glass dome.

Goldstein *et al.* (1993) in a rapidly rotating cylinder with non-slip boundary condition at the top and bottom and adiabatic boundary conditions on the side walls. In this study, the authors characterised two different types of convective mode at onset, labelled fast and slow. The fast modes correspond to motion at the edge of the cylinder. The slow modes describe convective patterns localised at the centre of the cylinder. Goldstein *et al.* (1993) also showed that the changeover between fast and slow modes is strongly dependent on the aspect ratio of the cylinder. On figure 4a, we observe a structure similar to a fast mode of azimuthal wavenumber $m = 2$. For this wavenumber Goldstein *et al.* (1993) predicted that the fast mode was the most unstable below an aspect ratio of 1.84, a condition satisfied in the TC geometry of our experiment.

For $R_c = 2.26$ (Fig. 4b), several columns are gathered around the centre of the Tangent Cylinder. These are reminiscent of structures which Aurnou *et al.* (2003) calls quasi-geostrophic modes, with the difference that in these authors' experiment, dye visualisations suggested that they were forming on the outside of the TC. When further increasing R_c ($R_c = 4.58$ Fig. 4c), we were able to see interaction between these central modes and "wall modes" forming near the side boundary. On figures 4d and 4e, we observe that, for $R_c \geq 6.29$ the central modes are merging into one larger structure, which evolves into a large central, retrograde vortex in the last stage of the convection observed in the experiment (figure 4f, $R_c = 11.27$).

The evolution towards a central retrograde vortex for critical parameters exceeding $R_c = 10$ was also found by Zhong *et al.* (1993) in experiments on convection in a rotating cylinder of aspect ratio $\Gamma = 1$ (hence wider than in the present case).

Figs. 5a to 5f show the flow at a smaller Ekman number, $E = 6.36 \times 10^{-6}$, for $R_c \in [0.35 \times Ra_c, 11.91 \times Ra_c]$. Near onset ($R_c = 1.35$, Fig. 5a),

the convective patterns are much smaller than for a comparable criticality at $E = 1.15 \times 10^{-5}$. When the criticality increases, we observe modes that correspond to the

modulated modes described by Goldstein *et al.* (1993). These feature spiralling arms (Fig. 5b) and were also observed experimentally by Zhong *et al.* (1993) for a comparable level of criticality ($R_c = 2.56$). Zhong *et al.* (1993) showed that these spiralling patterns arise from the outer wall of the cylinder as azimuthal mode. In the TC, we observe an azimuthal mode $m = 2$.

Such large differences between supercritical patterns at different Ekman numbers were theoretically predicted by Goldstein *et al.* (1993), whose analysis shows that when E is varied, the lowest critical Rayleigh number is alternately achieved with either a fast or a slow precessing mode. At higher criticality, convective patterns reflect a combination of wall modes and centre modes (at $R_c = 2.32, 4.40, 9.17$ on figures 5c, 5d and 5e), as for $E = 1.15 \times 10^{-5}$. Similarly to the more slowly rotating case too, convective patterns converge towards a central retrograde structure at the highest levels of supercriticality explored here (Fig. 5f).

For both values of E , the main features of the flow patterns (alternative presence of fast and slow modes at low levels of criticality depending on E and Γ , modulated modes, evolution towards a large retrograde vortex for $R_c \gtrsim 10$) supports the view that the convection in the Tangent Cylinder behaves as convection in a solid cylinder rather than in an infinite plane layer. It is also interesting to notice that the flow patterns discovered by Goldstein *et al.* (1993) and Zhong *et al.* (1993) at relatively high values of E remain dominant at the much lower values explored in our experiment. Such robustness may indicate that convection is in an asymptotic regime of rotation, as far as flow structures are concerned and that similar structures might also be found in the regimes of extreme rotation of the Earth for which $E \sim 10^{-15}$.

3.3. Evolution of the plume size and precession frequencies in supercritical regimes

The succession of supercritical patterns is reflected in the evolution of the dominating wavelengths and precession frequencies with criticality R_c , gathered on Fig. 6.

We find that beyond the onset of convection the dominating wavenumber follows a scaling of the form:

$$aE^{1/3} = (0.28 \pm 0.05) \times (R_c + 1)^{-0.2 \pm 0.03}. \quad (3.3)$$

This scaling extends the scaling for $a_c(E)$ found at the onset of convection to supercritical regimes. It expresses that as convection becomes more intense, the flow rearranges itself with fewer larger structures that are more efficient to carry the heat flux across the TC up to the point where only one structure is left for $R_c \gtrsim 10$.

The precession frequency first sharply increases in the weakly supercritical regime and subsequently saturates. It is nevertheless difficult to tell whether an asymptotic value is reached in the limit $R_c \rightarrow \infty$. Using a Landau model for the bifurcation, Goldstein *et al.* (1993) showed that in weakly supercritical regime, the precession normalised by Ω should vary as:

$$\omega_p = E^{-1}(\delta - \phi R_c) + O(R_c^2), \quad (3.4)$$

where the values of constant δ and ϕ depend on the aspect ratio of the cylinder (with $\delta \rightarrow 0$ in the limit of large aspect ratio to recover the non-overstable onset of convection in an infinitely extended plane layer Chandrasekhar (1961)).

The values of $\delta = 0.1$ and $\phi = 5$ were obtained experimentally by Zhong *et al.* (1993) and Ecke *et al.* (1992) for a cylinder of aspect ratio $\Gamma = 1$ and values of E greater than 10^{-3} . The variations of $\omega_p(r_c)$ extracted from experiments at several Ekman numbers

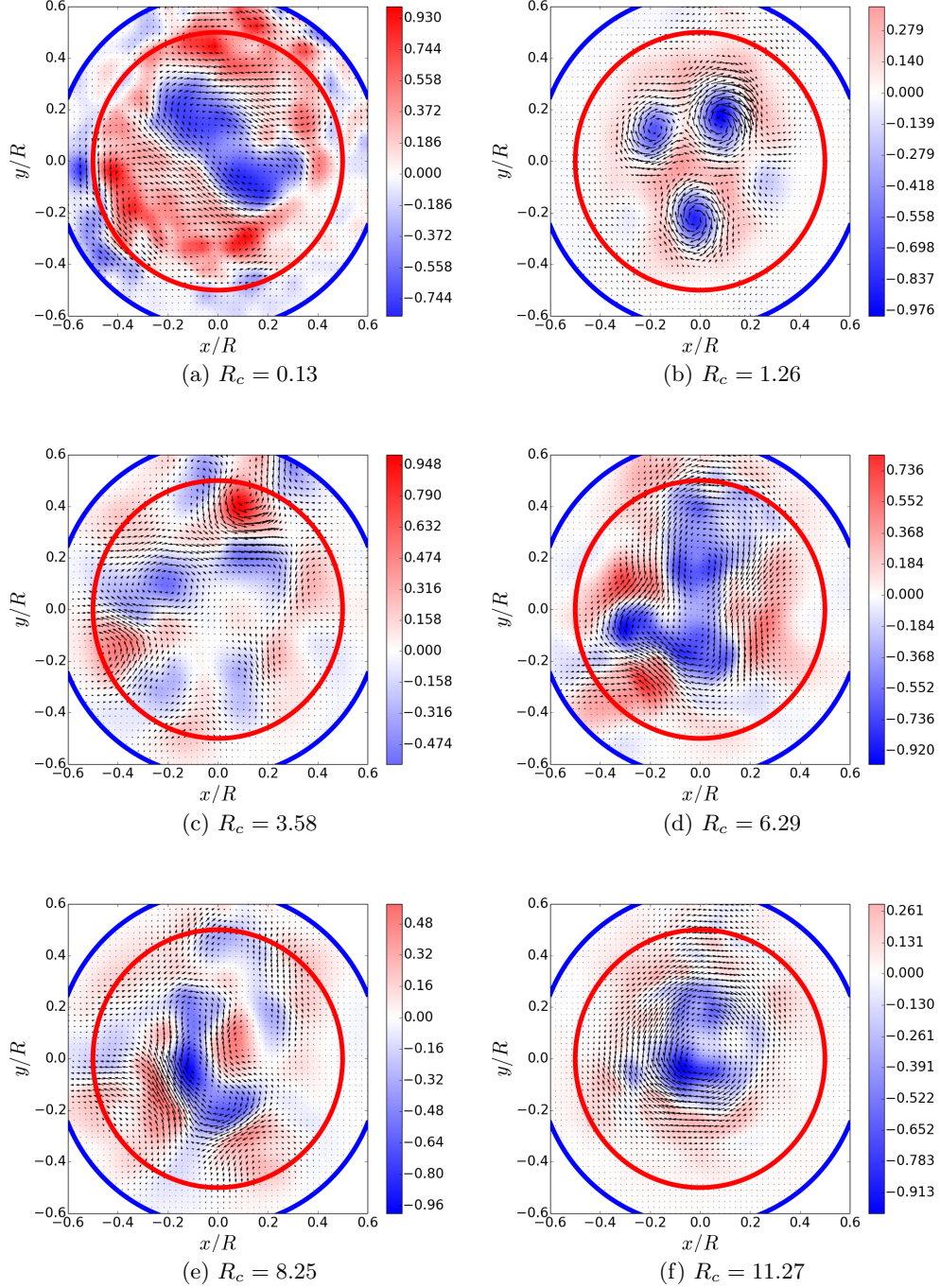


Figure 4: Time averaged velocity fields (arrows) with vorticity field (colorbar) in the horizontal plane for different Rayleigh numbers with $E = 1.15 \times 10^{-5}$. The blue line represents the boundary of the glass dome. The red line represents the position of the heater that defines the TC. The averaging time is 15 times smaller than the precession timescale $\tau_p = 2\pi/\omega_p$.

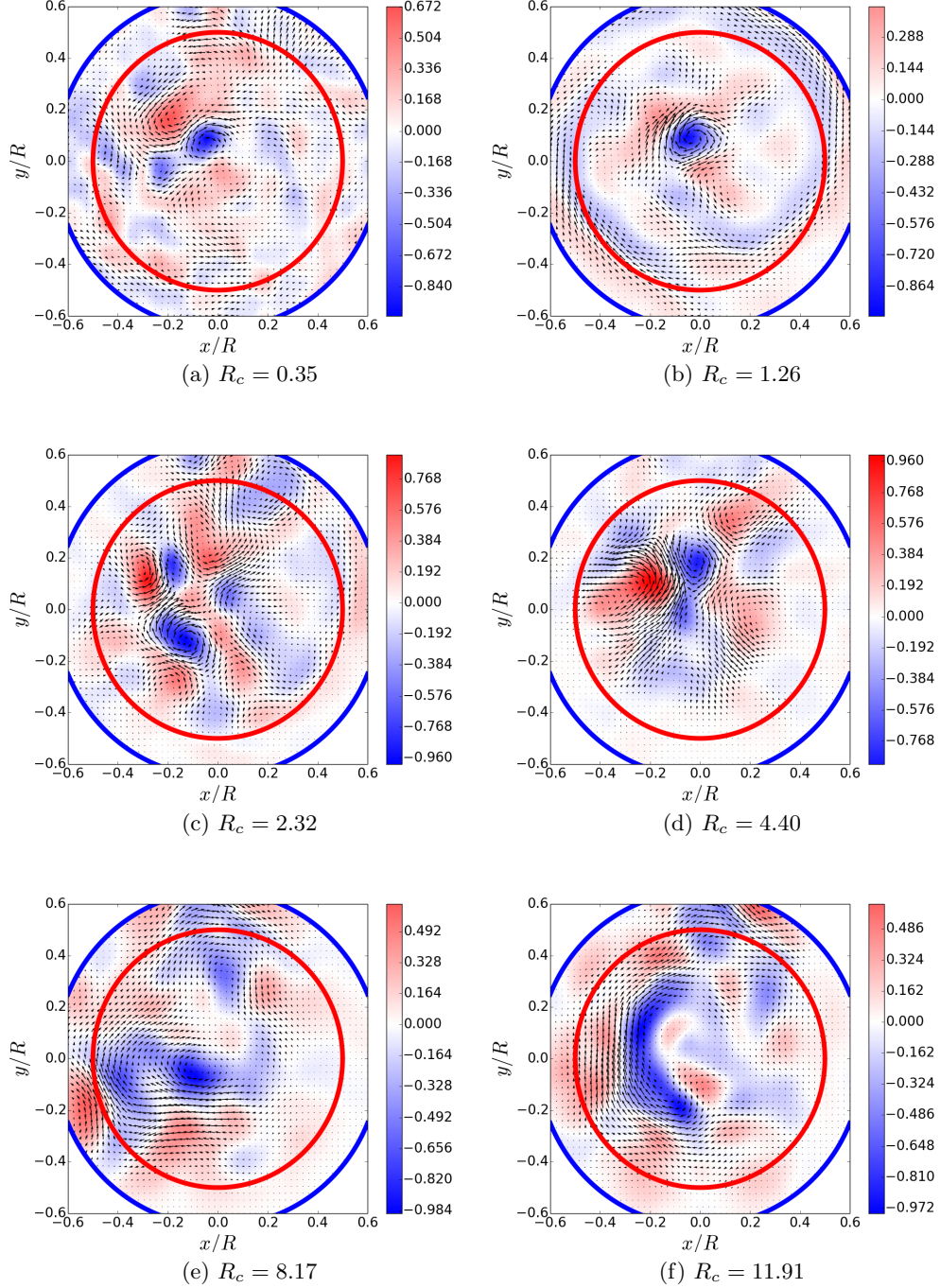


Figure 5: Time averaged velocity fields (arrows) with vorticity field (colorbar) in the horizontal plane for different Rayleigh numbers with $E = 6.36 \times 10^{-6}$. The blue line represents the boundary of the glass dome. The red line represents the position of the heater that defines the TC. The averaging time is 15 times smaller than the precession timescale $\tau_p = 2\pi/\omega_p$.

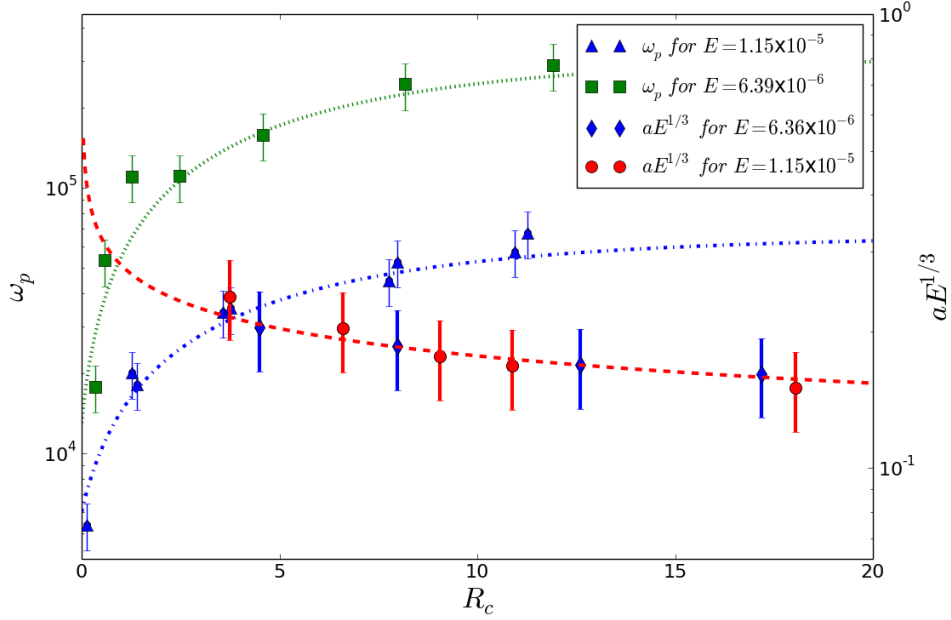


Figure 6: Evolution of the precession ω_p and the wave number a as function of the degree of criticality.

for $R_c > 0$ are reported on Fig. 6. They are best fitted over the widest measured range of values by an exponential law of the form:

$$\omega_p = (3 \pm 0.5) \times E^{-1} (1 - e^{(-0.15 \pm 0.01) \times R_c}) + \delta E^{-1}, \quad (3.5)$$

Expanding (3.5) to $\theta(R_c)$, and identifying with (3.4) we find that $\phi = 0.455 \pm 0.105$.

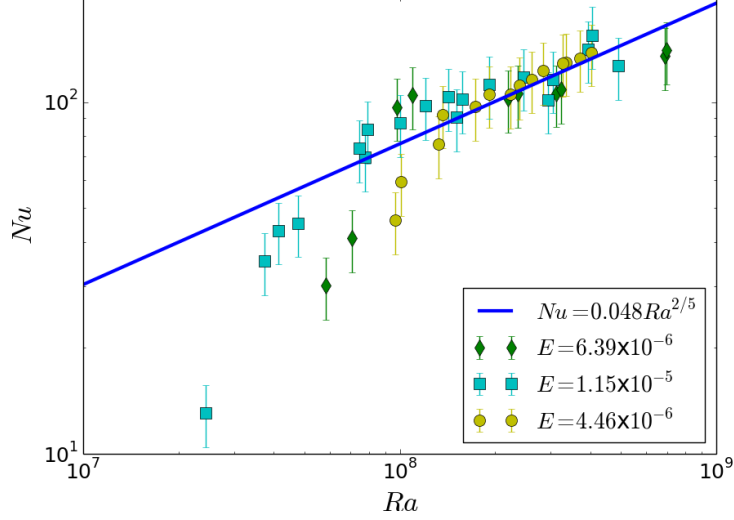
The value of δ is consistent with the findings of Ecke *et al.* (1992), but the supercritical variations of the precession frequency appear significantly slower than in the case of a solid rotating cylinder. It is however difficult to attribute this difference to either of the factors that differ between the two problems: the difference in shape of the upper domain boundary, a different aspect ratio, a three-order of magnitude difference in the Ekman number, different mechanical and thermal boundary conditions at the lateral boundary of the cylinder. Nevertheless, the precessing motion at onset and in supercritical regimes adds further support to the view that the phenomenology of convection in the tangent cylinder obeys the same mechanisms as in a solid rotating cylinder, both at the onset and in supercritical regimes.

4. Heat Flux and Thermal wind

4.1. Heat Flux through the Tangent Cylinder

Convection's efficiency is best measured through its ability to transport heat through the fluid layer.

In geophysical context, the heat transported through the CMB plays a crucial role as it is the main source of energy driving plate tectonics. Hence, we shall characterise the variations of the heat flux with Ra and E by means of the

Figure 7: Scaling of Nu vs. Ra

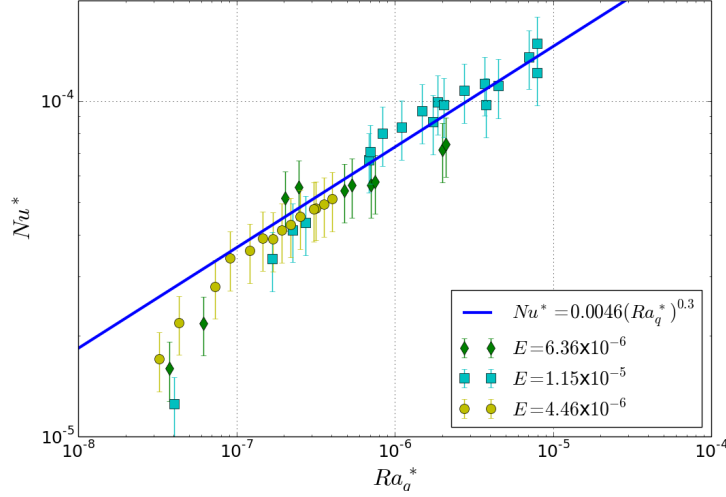
Nusselt number which represent the ratio of the heat flux in the fluid to the purely conductive flux:

$$Nu = \frac{Fd}{k\Delta T}, \quad (4.1)$$

where we recall that F is the heat flux through the top surface of the heater, obtained from the difference between the temperature of the heat-carrying fluid at the inlet and outlet of the heater,

and d is the height of fluid above the heater. The variations of Nu with Ra are reported on Fig. 7 for several values of E . All follow a scaling of the form $Nu = (0.048 \pm 0.004) \times Ra^{\frac{2}{5} \pm 0.05}$. A scaling with the same exponent was found in experiments by Sumita & Olson (2003), where convection was driven in a hemispherical shell, and theoretically predicted for that same geometry by Cardin & Olson (1994). In this configuration, however, although convective patterns resulted from the combined action of buoyancy and rotation, convection was driven by lateral heat flux out of the core at much lower critical Rayleigh numbers than in our tangent cylinder configuration (where lateral boundaries of the heater are practically adiabatic). In the spherical shell, convective patterns form Busse columns mostly outside the tangent cylinder Busse (1970). Nevertheless, both experiments operate in similarly low regimes of Ekman and Rossby numbers where the flow can be expected to be reasonably quasi-geostrophic. The fact that the same scaling holds for two very different convective patterns suggests that it may be a signature of quasi-geostrophic convection.

The comparison to previous studies can be furthered by inspecting how the heat flux normalised by rotation varies with the Rayleigh number based on the heat flux itself. One advantage of this approach is to quantify convection in terms of the available buoyancy. Buoyancy may indeed result from a heat flux at the boundary but also from a solute mass flux, as in the core of the Earth and other planets. On this basis, we follow Aubert *et al.* (2001); Aubert (2005); Christensen & Aubert (2006) and introduce the

Figure 8: Scaling of Nu^* vs. Ra_q^*

modified Nusselt number, Rayleigh number and a modified diffusionless Rayleigh number based on the heat flux:

$$Nu^* = Nu \times E \times Pr^{-1}, \quad (4.2)$$

$$Ra^* = Ra \times E^2 \times Pr^{-1}, \quad (4.3)$$

$$Ra_q^* = Ra^* Nu^*. \quad (4.4)$$

Christensen (2002), found that these quantities obeyed a scaling law of the form:

$$Nu^* \sim (Ra_q^*)^{5/9}. \quad (4.5)$$

This result was obtained with numerical simulations in a spherical shell geometry for $Ra_q^* \in [10^{-7}, 10^{-3}]$. Aurnou (2007) identified this scaling as indicative of a rapidly rotating regime.

Using Sumita & Olson (2003)'s data, this author also showed that for low values of Ra_q^* the relation between Nu^* and Ra_q^* was better fitted with a power law of the form $Nu^* \sim (Ra_q^*)^{0.29}$.

In the present configuration, Ra_q^* varies between 10^{-10} and 10^{-6} and therefore falls within a similar range to Sumita & Olson (2003)'s experiments. Collapsed data reported on Fig. 8 indeed obey a scaling close to that found by these authors:

$$Nu^* = (0.0046 \pm 0.0005) \times (Ra_q^*)^{0.3 \pm 0.02}. \quad (4.6)$$

Aurnou (2007) notes that this scaling appears in quasi-geostrophic regimes and indeed, the regime of parameters we explore corresponds to fast rotation and low flux-based Rayleigh number for which the flow is dominated by tall, quasi-geostrophic columns, as in Sumita & Olson (2003)'s experiments. Given the difference in geometry between our two setups, this scaling seems to mostly reflect this regime.

4.2. Thermal wind

In axisymmetric geometry, the balance between buoyancy and Coriolis forces gives rise to azimuthal motion, seen through the curl of the balance between these forces:

$$\frac{\partial u_\theta}{\partial z} \sim -\frac{g\beta}{2\Omega} \frac{\partial T}{\partial r}. \quad (4.7)$$

It follows that the largest retrograde motion is found in the higher latitudes, such as those of our PIV planes represented on figures 4 and 5 at a latitude of 51.5° . On the other hand, the direction of the thermal wind may reverse at low latitudes.

Hence, we extract from these measurements a radial profile of the azimuthal wind at two different latitudes (see figure 1) by means of an azimuthal and time average of the azimuthal velocity $\langle u_\theta(r, z) \rangle_{\theta t}$: one latitude corresponds to the polar region (51.5°) and the other to a plane close to the heater surface (20°). Results are plotted on figure 9a, 9b, 9c and 9d.

At high latitude (Figures 9a and 9b), the profiles exhibit a strong negative maximum followed by slightly positive values at larger radii, corresponding to a strong retrograde motion surrounded by a slightly prograde motion. Near the onset of convection, some prograde motion exists near the centre, that disappears as the flow becomes more supercritical. Despite the succession of different patterns observed in the supercritical regime, the intensity of the retrograde motion steadily increases with criticality.

For strongly supercritical flows ($R_c \gtrsim 11$), velocity patterns show a single structure slightly outgrowing the Tangent Cylinder (we shall see in section 5 that motion outside the TC does not necessarily imply that the Taylor-Proudman constraint is broken). This phenomenon appears for slightly higher criticality at higher values of E ($R_c \gtrsim 9$ at $E = 1.15 \times 10^{-5}$ and $R_c \gtrsim 11$ $E = 6.36 \times 10^{-6}$). In both cases, this confirms that in the most supercritical regimes, retrograde motion progressively invades the high-latitude region of the TC, where the flow becomes dominated by a large central retrograde vortex. Profiles of the region nearer the solid inner core provide a better picture of the three-dimensional structure of the solar wind (Figures 9c and 9d). In both cases, a prograde wind first develops near the solid core at low levels of criticality, and increases in intensity with R_c . At $E = 1.15 \times 10^{-5}$, the prograde wind starts weakening at the centre from $R_c = 2.37$ and starts becoming retrograde around $R_c = 9.92$. At higher rotation, weakening of the prograde wind near the solid core occurs only for $R_c > 9$, and we did not reach a regime where it reversed. This difference in levels of criticality for the weakening and reversal of the thermal wind near the solid core can be understood from the scaling for the critical Rayleigh number $Ra_c \sim E^{4/3}$ and (4.7) which imply that $\partial_z u_\theta \propto (R_c + 1)E^{1/3}$. Hence, thermal wind with a given vertical gradient of u_θ is expected to occur at for higher criticality when E is decreased.

Lastly, at clear azimuthal prograde jet is present at the edge of the Tangent Cylinder on the inside. The jet is thinner at faster rotation. It appears for $R_c \sim 2.37$ at $E = 1.15 \times 10^{-5}$ and $R_c \sim 4.06$ at $E = 6.36 \times 10^{-6}$, and slightly increases with criticality. One cannot but notice the similarity between this structure and the non-axisymmetric azimuthal jets near the TC inferred by Livermore *et al.* (2017) from satellite measurements of the Earth magnetic field. Nevertheless, although the forces driving the jet remain unknown, the authors suggest that they are most likely of magnetic origin, an effect that is absent in the present study.

Lastly, we shall quantify the intensity of the thermal wind in terms of the Rossby

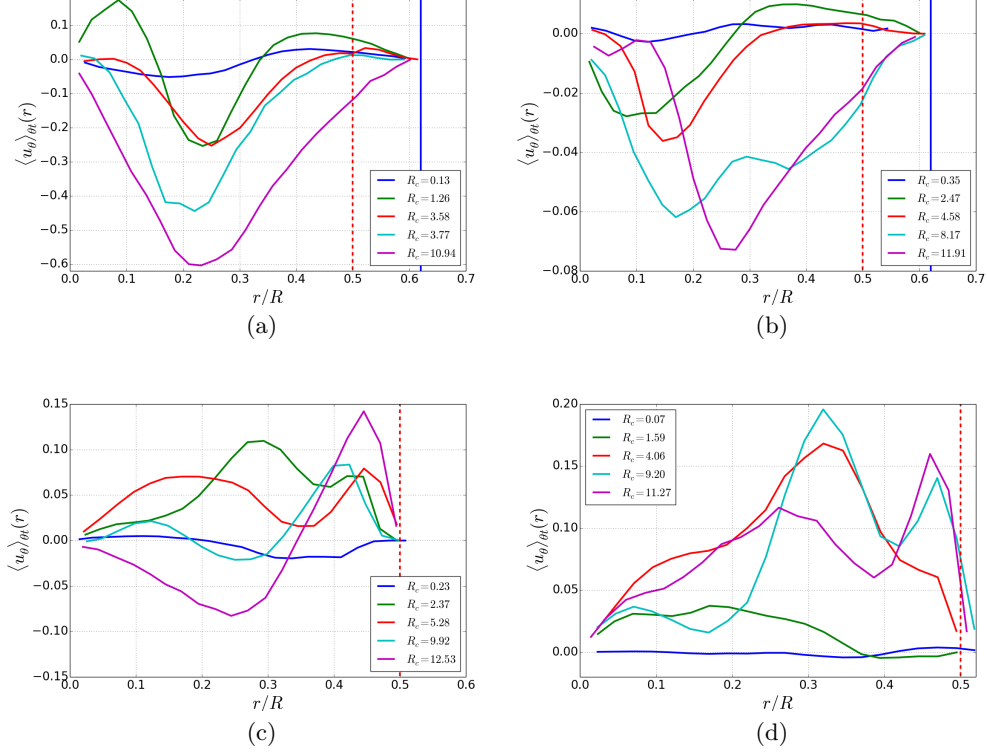


Figure 9: Azimuthally and time-averaged radial profiles of azimuthal velocities $\langle u_\theta \rangle_{\theta t}(r)$, for several levels of criticality. Top: data from horizontal plane at 51.5° . Bottom, data from horizontal plane at 20° . Left $E = 1.15 \times 10^{-5}$, Right: $E = 6.36 \times 10^{-6}$. Vertical dashed line: TC boundary, vertical solid line: position of the glass dome.

number, Ro , and its variations with the diffusionless flux Rayleigh number, Ra_q^* . The Rossby number, defined as

$$Ro = \frac{U_m}{2R\Omega} \quad (4.8)$$

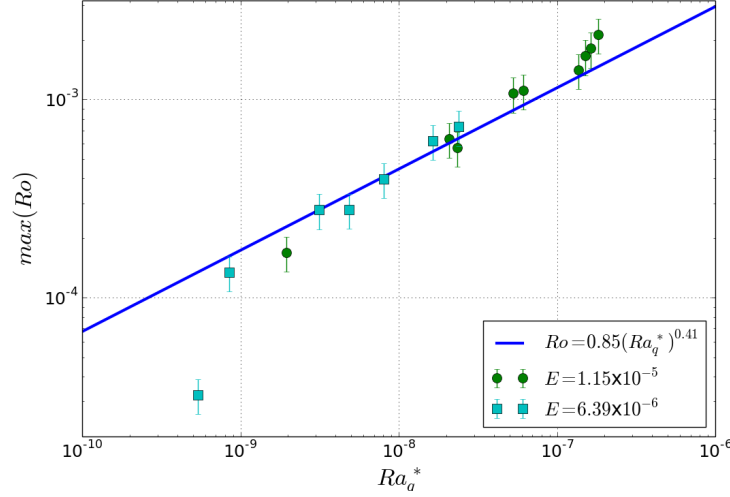
measures the ratio of inertia to the Coriolis force, where U_m is chosen as the maximum retrograde velocity in the averaged profiles of the thermal wind measured in the high latitude plane reported on figures 9a and 9b.

Our results, reported on figure 10, obey the scaling

$$Ro = 0.85 \times (Ra_q^*)^{0.41 \pm 0.02}. \quad (4.9)$$

This scaling is very close to the $Ro \sim (Ra_q^*)^{0.4}$ law, which Cardin & Olson (1994) first derived in a spherical geometry, from the conservation of potential vorticity and under the assumption of quasi-geostrophy. This scaling was also experimentally verified by Aubert *et al.* (2001) by means of measurements of azimuthal velocities in a spherical shell.

This suggests that despite differences in geometry, the azimuthal wind in the TC is

Figure 10: Scaling of Ro vs. Ra_q^*

also governed by a quasi-geostrophic balance. Hence, the behaviour of the thermal wind concurs with that of the heat flux to suggest that the convective regimes we observe are dominated by rotation.

5. Effect of the confinement

The structure of convection, and the scalings for the heat flux and the thermal wind draw a picture of convection within the TC at low Ekman numbers that is quasi-geostrophic and resembles convection in a cylinder confined by solid walls. Both features reflect a prominent role of background rotation and the TP constraint it imposes on the flow. Based on these observations, shall conclude this study by measuring the degree of confinement within the TC. Figures 11a and 11c respectively show the z -RMS profiles of vertical and radial velocities for $E = 1.15 \times 10^{-5}$. The radial velocity at the side boundary of the TC never exceeds a few percents of its typical value within the TC so the TP constraint can be seen as enforcing a near-impermeable condition there. For low criticality, vertical fluid motion too is entirely contained within the radius of the TC. For $R_c \geq 6.41$, however, a slight motion appears outside the TC, that remains at approximately the same level as R_c is increased. The same is true for the azimuthal wind, which extends slightly beyond the TC at moderate to high levels of criticality (Figs. 9a and 9c). Vertical and azimuthal motion do not, however, directly break the break the TP constraint. Momentum inside the TC is indeed transported across the TC boundary by viscous friction. Friction is all the more effective there as a fee Stewartson layer is expected to develop there, with a inner thickness scaling as $E^{-1/3}$ and an outer thickness scaling as $E^{-1/4}$ Stewartson (1957); Fröh & Read (1999). Such layers are too thin to be reasonably detected in our measurements. Nevertheless, the radial profiles of azimuthal velocities on figure 9a- 9d show hint of a variation in slope across the TC boundary. This local slope is also considerably steeper at $E = 6.36 \times 10^{-6}$ than $E = 1.15 \times 10^{-5}$. This suggests that the mechanical condition across the TC boundary is probably closer to one of imposed tangential stress rather than the no-slip condition of a rigid boundary. This tendency is confirmed by the z -RMS profiles of vertical and radial velocities for

$E = 6.36 \times 10^{-6}$. For this faster rotation, the radial velocity is found to be exactly zero at the boundary of the TC at all levels of criticality, within the precision of our measurements. Vertical velocity is also practically zero. The convection even seems extinct on the last 20% of the TC's outer region. Clearly this behaviour is promoted by the fact that the hot boundary of the domain is itself confined within the domain. However, the intense convection that ensues would not remain confined within the higher latitudes of the TC without a strong influence of the TP constraint. Overall, the behaviour is similar to that found at $E = 1.15 \times 10^{-5}$, except that the TP constraint is more strictly enforced at equivalent levels of criticality.

The confinement effect is further slightly reinforced by the curvature of the dome, which incurs a variation of height of 7.8% between the centre and the edge of the TC. This geometry has two consequences: first, the Rayleigh number based on the local fluid height is 25% lower at the edge of the TC than in the middle, so convection is favoured there. Indeed, the centre of the TC is the location where convection is first detected (see lowest values of R_c on figure 11a and 11b). It also remains more intense there in the supercritical regimes. Second, the associated TP constraint opposes radial motion which slightly reinforces confinement. In planetary cores, the spherical shape of the solid core reverses the radial variation of height compared to our experiment but it similarly opposes radial motion, thus reinforcing confinement too. In both cases, however the confinement associated to this effect can be expected to be of significantly less influence than the TP constraint incurred at the outside edge of the TC.

6. Conclusions and discussion

The experimental study we conducted was focused on convection in a Tangent Cylinder for Ekman numbers in the range 3.36×10^{-6} to 4.51×10^{-5} , and brought several answers to the four questions set in the introduction:

First, the critical scalings for the onset of convection in a TC are similar to those known for plane convection, albeit with different constants: the critical Rayleigh number $Ra_c = (26 \pm 4) \simeq E^{4/3 \pm 0.1}$ is marginally higher, but the critical wavenumber $a_c = (0.5 \pm 0.07) \times E^{-1/3 \pm 0.05}$ is significantly higher than for plane convection.

Second, this discrepancy finds its root in the structure of the critical convective plumes, which resemble those found in rotating cylinders, rather than the periodic cell pattern of plane rotating convection. As in the former, the critical mode is either one of the slow or one of the fast modes identified by Goldstein *et al.* (1993), depending on the Ekman number and the aspect ratio of the cylinder.

Third, the loss of translational symmetry in the horizontal plane excludes an onset of convection through steady modes, even at the moderate values of Pr for which these modes are found in the plane configuration rather than travelling waves that characterise over-stability in a plane configuration, however, the time-dependence takes the form a very slow retrograde precession.

Fourth, the supercritical regimes exhibit a complex sequence of convective patterns, leading to a single, large vortex centred on the cylinder axis when the Rayleigh number exceeds approximately 10 times the critical value. In the high latitudes, this vortex translates into a coherent, retrograde thermal wind. For the Ekman numbers we considered, the intensity of the thermal wind, measured in terms of the Rossby number obeys a scaling of $Ro = 0.85 \times (Ra_q^*)^{0.41}$ identical to the scaling found by Aubert (2005); Christensen & Aubert (2006) found for the convection outside the TC. It reflects a dynamics driven by the conservation of potential vorticity in the quasi-geostrophic-regime. This phenomenol-

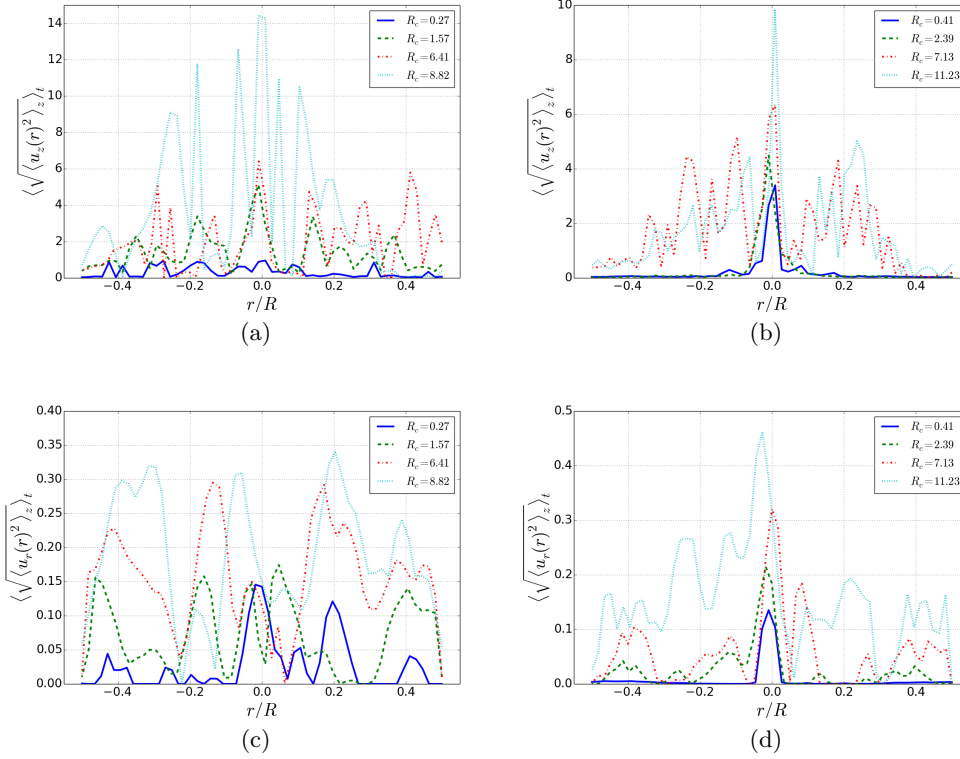


Figure 11: (a) and (c) $\langle \sqrt{\langle u_z(r)^2 \rangle_z} \rangle_t$ (top) and $\langle \sqrt{\langle u_r(r)^2 \rangle_r} \rangle_z$ (bottom) for several increments of supercriticality and $E = 1.15 \times 10^{-5}$. (b) and (d) Similarly, $\langle \sqrt{\langle u_z(r)^2 \rangle_z} \rangle_t$ and $\langle \sqrt{\langle u_r(r)^2 \rangle_r} \rangle_z$ for several increments of supercriticality and $E = 6.36 \times 10^{-6}$.

ogy is supported by the scaling for the heat flux $Nu^* = (0.0046 \pm 0.0005) \times (Ra_q^*)^{0.3 \pm 0.02}$, which is also found in quasi-geostrophic regimes.

Fifth, the geometry of the flow in the vicinity of the TC lateral boundary confirms that the Taylor-Proudman constraint is practically not broken there. On the other hand, for intense enough convection, the likely Stewartson layers that develop along these boundary diffuse a small part of the momentum inside the TC towards regions outside it.

Finally, since our work has been mostly motivated by the study of planetary cores, it is tempting to try and gain insight on their dynamics from these conclusions. This endeavour however meets several important obstacles. The first is the difference in working fluids. The liquid core of the Earth operates in a regime of low Prandtl number and extreme rotation for which the onset of convection would be overstable, even in plane configuration. Nevertheless It is still reasonable to expect that confinement within the TC induced by the virtual boundaries raised by the TP constraint reshape convection in a similar way as it does at the moderate Prandtl numbers considered in this paper, for which no overstability occurs. This view is supported by the linear stability analysis of convection in a rotating cylinder at low Prandtl numbers by Goldstein *et al.* (1994), which shows that the critical modes are subject to both precession and overstability oscillations. Furthermore, convection in the Earth core is also compositional in nature, rather

than only thermal. The corresponding Schmidt numbers are in a range comparable to the thermal Prandtl numbers of water and acid, for which the onset of convection would not be overstable. Still, a deeper understanding of convection in a TC a low Prandtl number would require liquid metal experiments in a configuration similar to the present paper. The second obstacle is raised by electromagnetic forces induced by the Earth magnetic field, which can potentially change the structure of convection in the core in a radical way. Typically these forces favour larger, and more unstable plumes Aujogue *et al.* (2015). However, electromagnetic forces are also likely to prevent overstability. Hence, it is hoped that magnetoconvection experiments in a TC configuration at moderate Prandtl number (which our apparatus was designed to perform) could provide us with a somewhat more realistic picture of convection in the core than rotating convection alone.

REFERENCES

- AUBERT, JULIEN 2005 Steady zonal flows in spherical shell dynamos. *Journal of Fluid Mechanics* **542**, 53–67.
- AUBERT, JULIEN, BRITO, DANIEL, NATAF, HENRI-CLAUDE, CARDIN, PHILIPPE & MASSON, JEAN-PAUL 2001 A systematic experimental study of rapidly rotating spherical convection in water and liquid gallium. *Physics of the Earth and Planetary Interiors* **128** (1), 51–74.
- AUJOGUE, KELIG, POTHERAT, ALBAN, BATES, IAN, DEBRAY, FRANCOIS & SREENIVASAN, BINOD 2016 Little earth experiment: An instrument to model planetary cores. *Review of Scientific Instruments* **87** (8), 084502.
- AUJOGUE, KELIG, POTHERAT, ALBAN & SREENIVASAN, BINOD 2015 Onset of plane layer magnetoconvection at low ekman number. *Physics of Fluids* **27** (10), 106602.
- AURNOU, JM 2007 Planetary core dynamics and convective heat transfer scaling. *Geophysical and Astrophysical Fluid Dynamics* **101** (5-6), 327–345.
- AURNOU, J., ANDREADIS, S., ZHU, L. & OLSON, P. 2003 Experiments on convection in Earth's core tangent cylinder. *Earth Planet. Sci. Lett.* **212** (1), 119–134.
- BUSSE, F. H. 1970 Thermal instabilities in rapidly rotating systems. *J. Fluid Mech.* **44** (03), 441–460.
- CARDIN, PHILIPPE & OLSON, PETER 1994 Chaotic thermal convection in a rapidly rotating spherical shell: consequences for flow in the outer core. *Physics of the earth and planetary interiors* **82** (3-4), 235–259.
- CHANDRASEKHAR, S. 1961 *Hydrodynamic and hydromagnetic stability*. Clarendon Press, Oxford.
- CHRISTENSEN, UR 2002 Zonal flow driven by strongly supercritical convection in rotating spherical shells. *Journal of Fluid Mechanics* **470**, 115–133.
- CHRISTENSEN, UR & AUBERT, JULIEN 2006 Scaling properties of convection-driven dynamos in rotating spherical shells and application to planetary magnetic fields. *Geophysical Journal International* **166** (1), 97–114.
- CLUNE, T. & KNOBLAUCH, E. 1993 Pattern selection in rotating convection with experimental boundary conditions. *Phys. Rev. E* **47** (4), 2536–2540.
- ECKE, RE, ZHONG, FANG & KNOBLOCH, E 1992 Hopf bifurcation with broken reflection symmetry in rotating rayleigh-bénard convection. *EPL (Europhysics Letters)* **19** (3), 177.
- FRÜH, W.-G. & READ, P. 1999 Experiments on a barotropic rotating shear layer. part 1. instability and steady vortices. *J. Fluid Mech.* **383**, 143–173.
- GOLDSTEIN, H.F., KNOBLAUCH, E., MERCADER, I. & NET, M. 1994 Convection in a rotating cylinder. part 2. linear theory for low prandtl numbers. *J. Fluid Mech.* **262**, 293–324.
- GOLDSTEIN, HF, KNOBLOCH, E, MERCADER, I & NET, M 1993 Convection in a rotating cylinder. part 1 linear theory for moderate prandtl numbers. *Journal of Fluid Mechanics* **248**, 583–604.
- LIVERMORE, P.W., HOLLERBACH, R. & FINLAY, C. 2017 An accelerating high-latitude jet in earths core. *Nat. Geo.* **10**, 62–69.
- MAXWORTHY, T. & NARIMOUSA, S. 1994 Unsteady turbulent convection into a homogeneous rotating fluid with oceanic applications. *J. Phys. Ocean.* **24**, 865–887.

- SCHUBERT, G. & SODERLUND, K.M. 2011 Planetary magnetic fields: Observations and models. *Physics of the Earth and Planetary Interiors* **187** (3), 92–108.
- SREENIVASAN, B. & JONES, C. A. 2006 Azimuthal winds, convection and dynamo action in the polar regions of planetary cores. *Geophys. Astrophys. Fluid Dyn.* **100** (4-5), 319–339.
- STEWARTSON, K. 1957 On almost rigid rotations. *J. Fluid Mech.* **3**.
- SUMITA, IKURO & OLSON, PETER 2003 Experiments on highly supercritical thermal convection in a rapidly rotating hemispherical shell. *Journal of Fluid Mechanics* **492**, 271–287.
- ZHONG, FANG, ECKE, ROBERT E & STEINBERG, VICTOR 1993 Rotating rayleigh–bénard convection: asymmetric modes and vortex states. *Journal of Fluid Mechanics* **249**, 135–159.